High-Temperature Oxidation of High-Entropy FeNiCoCrAl Alloys

GUMEN Olena [1, a] *, KARPETS Myroslav [2, b], SMAKOVSKA Ganna [3, c]
and YAKUBIV Mykola [4, d]

[1] National Technical University of Ukraine "Igor Sikorsky Kyiv Polytechnic Institute", 37 Peremohy Avenue, Kyiv, 03056, Ukraine, ORCID: 0000-0003-3992-895X,

[2] National Technical University of Ukraine "Igor Sikorsky Kyiv Polytechnic Institute", Kyiv, Ukraine, ORCID: 0000-0001-9528-1850

[3] National Technical University of Ukraine "Igor Sikorsky Kyiv Polytechnic Institute", Kyiv, Ukraine, ORCID: 0000-0003-3900-4431

[4] National Technical University of Ukraine "Igor Sikorsky Kyiv Polytechnic Institute", Kyiv, Ukraine

[a] gumens@ukr.net, [b] mkarpets@ukr.net, [c] anna-07@ukr.net, [d] fmf_ikg@ukr.net

Keywords: High-Entropy Alloy, Valence Electron Concentration, Oxidation, Solid Solution, Ordering, Automated Indentation, Hardness, Microstructure

Abstract. Phase composition and mechanical properties and the formation of oxide layers on $Fe_{40-x}NiCoCrAl_x$ (x = 5 and 10 at.%) alloys in long-term oxidation at 900 and 1000°C were studied. In the initial cast state, depending on the aluminum content and valence electron concentration, the alloys contain only an fcc solid solution (VEC = 8 e/a) or a mixture of fcc and bcc phases (VEC = 7.75 e/a). Thin continuous oxide scales containing Cr_2O_3 and $NiCr_2O$ spinel formed on the surface of both alloys oxidized at 900°C for 50 h. A further increase in the annealing time to 100 h leads to the formation of aluminum oxide Al_2O_3 in the scale on the $Fe_{30}Ni_{25}Co_{15}Cr_{20}Al_{10}$ alloy, having high protective properties. An increase in the oxidation temperature to 1000°C results in partial failure of the protective layer on the alloy with 10 at.% Al. Long-term holding at 900°C (100 h) + 1000°C (50 h) does not change the phase composition of the $Fe_{35}Ni_{25}Co_{15}Cr_{20}Al_5$ alloy matrix, being indicative of its high thermal stability. In the two-phase $Fe_{30}Ni_{25}Co_{15}Cr_{20}Al_{10}$ alloy, the quantitative ratio of solid solutions sharply changes: the amount of the bcc phase increases from 4 to 54 wt.% and its B2-type ordering is observed. The mechanical characteristics of the starting alloys and those after long-term high-temperature annealing were determined by automated indentation. The hardness (HIT) and elastic modulus (E) of the cast $Fe_{35}Ni_{25}Co_{15}Cr_{20}Al_5$ alloy are equal to 2 and 147 GPa, respectively, and decrease to 1.8 and 106 GPa after a series of long-term annealing operations. The $Fe_{30}Ni_{25}Co_{15}Cr_{20}Al_{10}$ alloy shows the opposite dependence: HIT increases from 2.5 in the initial state to 3.1 GPa after annealing and E decreases from 152 to 134 GPa. This indicates that the $Fe_{30}Ni_{25}Co_{15}Cr_{20}Al_{10}$ alloy is promising as a high-temperature oxidation-resistant and creep-resistant material.

Introduction

A new class of alloys, called high-entropy alloys (HEAs), possessing low free energy and high mixing entropy has been of research focus recently. They contain more than four elements in an equiatomic or close ratio (Yeh et al., 2004). The HEAs are peculiar in that they form simple substitutional solid fcc or bcc solutions or a mixture of bcc + fcc solid solutions (Gao et al., 2013; Sheng et al., 2011). Differently doped alloys in which simple bcc and fcc solid solutions form are among HEAs that have been studied most extensively. Numerous papers focus on the optimization of alloy structures and mechanical properties (Firstov et al., 2013ab; Firstov et al., 2016a; Gumen et al., 2019ab; Wang et al., 2012). There are currently very limited data on the high-temperature

oxidation resistance of these materials and the stability of their phase composition and mechanical properties in long-term high-temperature holding (Butler et al., 2016ab; Holcomb et al., 2015; Kim et al., 2018; Wu et al., 2017). Our objective is to examine the effect of aluminum on the stability of phase composition, structure, and mechanical properties and on the formation of oxide layers in long-term temperature oxidation of the $Fe_{40-x}NiCoCrAl_x$ alloys (x = 5 and 10 at.% Al) at 900 and 1000°C.

Experimental part

The $Fe_{40-x}NiCoCrAl_x$ alloys (x = 5 and 10 at.% Al) were produced by arc melting in a high-purity argon atmosphere. The ingots were melted six to seven times to homogenize their composition. The starting components were high-purity materials (at least 99.98% purity).

The oxidation resistance of the alloys was examined in an electric arc furnace at 900 and 1000°C in air. The samples were periodically weighed in 5, 10, 25, 50, and 100 h. To measure the weight change of the samples, we used a Radwag precision balance (±0.0001 g). The oxidation resistance was assessed from the specific change in weight of the samples q ($mg/cm^2 \cdot h$).

The phase composition of the starting alloys and those after high-temperature oxidation was analyzed with an Ultima IV diffractometer in monochromatic Cu-K_α radiation. The X-ray diffraction data were processed using the PowderCell 2.4 software for full-profile analysis of X-ray spectra for a mixture of polycrystalline phase components. The accuracy of the measured lattice period values is ±0.0001 nm. The morphology and microstructure of scales on the starting and annealing alloys were examined with a Jeol Superprobe 733 scanning electron microscope (SEM) and with a MIM-8 optical microscope. The mechanical properties were determined by automated indentation with a Berkovich pyramid under 3N load employing a Micron Gamma unit.

Results and Discussion

The fcc solid-solution phase is known (Butler et al., 2017; Firstov et al., 2016b) to form at elevated valence electron concentrations, VEC ≥ 8 e/a, in high-entropy alloys in most cases, while the bcc solid-solution phases are stable at VEC ≤ 6.87 e/a. If the valence electron concentration is 7.2 ≤ VEC ≤ 8 e/a, a mixture of two, bcc and fcc, solid solutions forms. According to our calculations, VEC = 8 e/a for the $Fe_{35}Ni_{25}Co_{15}Cr_{20}Al_5$ alloy and 7.75 e/a for the $Fe_{30}Ni_{25}Co_{15}Cr_{20}Al_{10}$ alloy (Table 1).

Table 1.   *Phase Constituents of the Cast Alloys, Lattice Parameters of the Phases, and Valence Electron Concentrations*

Alloy	Phase constituents, wt.%	Lattice parameter a, nm	VEC, e/a
$Fe_{35}Ni_{25}Co_{15}Cr_{20}Al_5$	100 FCC	0,3571	8
$Fe_{30}Ni_{25}Co_{15}Cr_{20}Al_{10}$	96 FCC 4 BCC	0,3603 0,2862	7,75

Metallographic analysis of the high-entropy alloys in starting (cast) state showed that the $Fe_{35}Ni_{25}Co_{15}Cr_{20}Al_5$ microstructure (Fig. 1b) included grains elongated in the crystallization direction and subgrains at grain boundaries and partially inside them. With higher aluminum content of the $Fe_{30}Ni_{25}Co_{15}Cr_{20}Al_{10}$ alloy, dendritic crystallization leading to light dendrites and a darker phase in the space between the dendrites was observed (Fig. 1d).

A greater aluminum content of the alloy reduces VEC, in turn indicating that stability of the fcc solid solution reduces and the bcc phase forms through solid-phase decomposition mechanism.
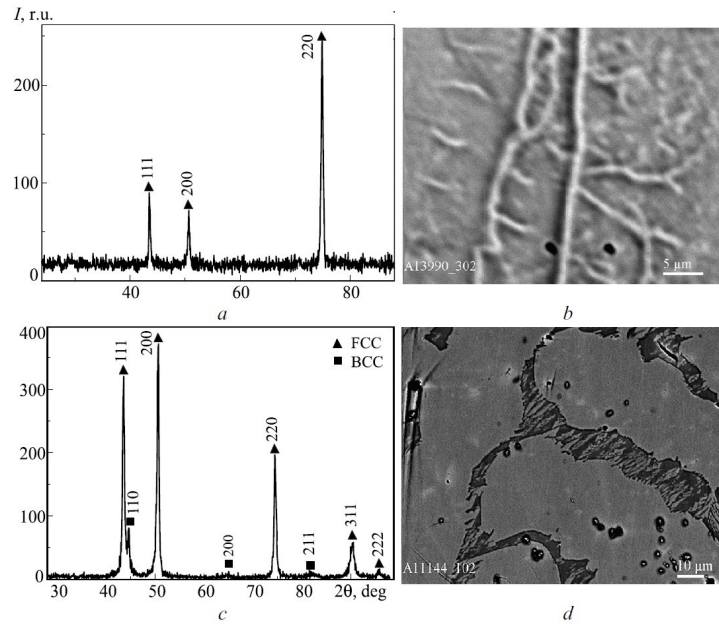

Fig. 1. *X-ray diffraction patterns (a, c) and microstructures (b, d) for the Fe$_{35}$Ni$_{25}$Co$_{15}$Cr$_{20}$Al$_5$ (a, b) and Fe$_{30}$Ni$_{25}$Co$_{15}$Cr$_{20}$Al$_{10}$ (c, d) high-entropy alloys in starting state (SEM).*

Figure 2 shows variation in the specific weight of the samples q (mg/cm^2) after oxidation of the Fe$_{35}$Ni$_{25}$Cr$_{20}$Co$_{20}$Al$_5$ and Fe$_{30}$Ni$_{25}$Cr$_{20}$Co$_{15}$Al$_{10}$ high-entropy alloys at 900ºC for 100 h and then at 1000°C for 50 h. After short holding for 5 h at 900°C, the specific weight of the alloy samples increased differently. The alloy with 10 at.% Al oxidized much more slowly for the first 5 h than the alloy containing 5 at.% Al.
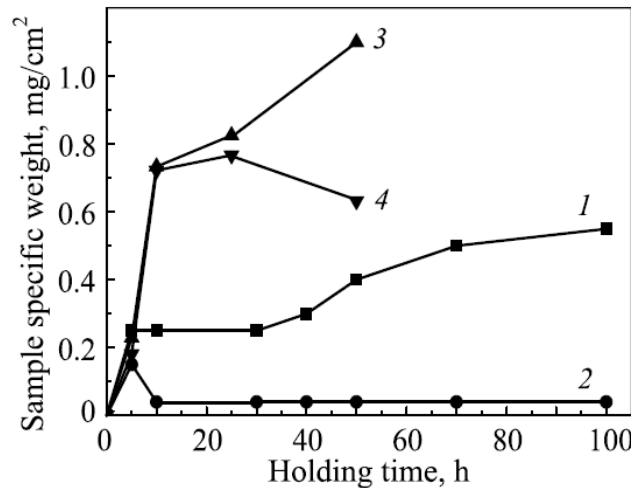

Fig. 2. *Variation in the specific weight of alloy samples after oxidation at 900°C (100 h) and further at 1000°C (50 h).*

The specific weight of the Fe$_{35}$Ni$_{25}$Cr$_{20}$Co$_{20}$Al$_5$ alloy showed a stable gain for 30 h at 900°C and naturally increased further with longer holding as oxide film began to develop and grow. The Fe$_{30}$Ni$_{25}$Cr$_{20}$Co$_{15}$Al$_{10}$ alloy behaved differently. The sample significantly gained weight after the

first 5 h and then partially lost its weight, which was accompanied by the formation of a thin brittle scale that spalled in some places. A dense scale formed further and oxidation proceeded not only without weight losses but also without weight gain, being indicative of high protective properties of the oxide film. However, a further increase of the oxidation temperature to 1000°C led to a sharp gain in the specific weight of the samples and growth of the scale thickness (Fig. 2).

The $Fe_{35}Ni_{25}Cr_{20}Co_{20}Al_5$ alloy showed a continuous increase in the specific weight within entire holding at 1000°C; q was minimum for the first 5 h and the oxidation rate sharply increased in a period between 5 to 10 h. During the next exposure in the interval from 10 to 25 hours, a significant slowdown in the oxidation process is observed, and then there is a significant increase in the increase in the mass of the samples, this may indicate that the scale formed on the surface of the alloy does not have high protective properties at a given temperature.
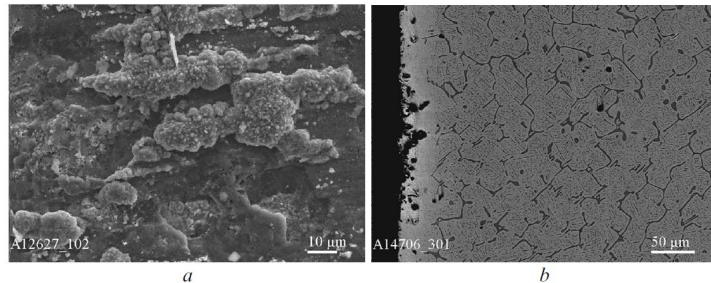

Fig. 3. *Morphology of the scale on the $Fe_{30}Ni_{25}Cr_{20}Co_{15}Al_{10}$ alloy (a) after oxidation at 900°C (100 h) + 1000°C (50 h) and cross-sectional microstructure (b).*

The situation was different for the $Fe_{30}Ni_{25}Cr_{20}Co_{15}Al_{10}$ alloy that contained more aluminum and less iron. After the first 5 h, the sample weight gain was much lower than that of the $Fe_{35}Ni_{25}Cr_{20}Co_{20}Al_5$ alloy. In a period between 5 and 10 h, q substantially increased and then (10–25 h) the process sharply slowed down. In a period between 25 and 50 h, the curve showing variation in the specific weight changed its direction. When the sample cooled down, the scale partially spalled since the protective film failed under a cyclic change in temperatures because of different thermal expansion coefficients (TECs) of the scale and alloy matrix (Fig. 3).

A two-phase oxide film containing Cr_2O_3 and $NiCr_2O_4$ spinel formed on both alloys at 900°C for 50 h. The scales were very thin (3–5 μm thick on the $Fe_{30}Ni_{25}Cr_{20}Co_{15}Al_{10}$ alloy and 7–8 μm thick on the $Fe_{35}Ni_{25}Cr_{20}Co_{20}Al_5$ alloy) and the X-ray diffraction patterns of both alloys had also reflections from the matrix phase of the fcc solid solution (Fig. 4).

The lattice parameter of the fcc solid solutions in the $Fe_{35}Ni_{25}Cr_{20}Co_{20}Al_5$ alloy increased compared to the starting state and became a = 0.3577 nm (since the near-surface metal layer was saturated with oxygen) and that in the $Fe_{30}Ni_{25}Cr_{20}Co_{15}Al_{10}$ alloy substantially decreased and became a = 0.3585 nm (Table 2), indicating that metal ions diffused toward the oxidation front. Some diffusion processes occurred under the scale. For example, the aluminum diffusion rate increased with temperature. Hence, the aluminum concentration toward the metal surface became higher to promote the formation of Al_2O_3. In turn, this indicates that the fcc phase became depleted of aluminum and its lattice parameter decreased.

The amount of the fcc phase in the 5 at.% Al alloy was 7 wt.% and that in the 10 at.% Al alloy was 41 wt.%. This substantial difference can be attributed to varying thickness of the scales; as a result, X-rays penetrate to different depths of the sample. The main phase of the scales is presented by oxides of Cr_2O_3 structure: their amount reaches 83 wt.% for $Fe_{35}Ni_{25}Cr_{20}Co_{20}Al_5$ and 42 wt.% for $Fe_{30}Ni_{25}Cr_{20}Co_{15}Al_{10}$.

The amount of $NiCr_2O_4$ spinel in the scale of the $Fe_{35}Ni_{25}Cr_{20}Co_{20}Al_5$ alloy was 10 wt.% and that in the $Fe_{30}Ni_{25}Cr_{20}Co_{15}Al_{10}$ alloy was 17 wt.%. Further holding changed the scale phase

composition. The alloy with lower aluminum content had a scale after 100 h at 900°C containing two phases: $Cr_{13}Fe_7O_{30}$ and $NiCr_2O_4$ (Fig. 4b).

The presence of $Cr_{13}Fe_7O_{30}$ can be explained by the fact that iron oxidized in long-term holding to form FeO that dissolved in Cr_2O_3 to create the $Cr_{13}Fe_7O_{30}$ phase with lattice parameters a = 0.4986 nm and c = 1.3646 nm, which is isostructural to Cr_2O_3.

The $NiCr_2O_4$ lattice parameter increased after oxidation at 900°C and became 0.8350 nm (Table 2). In oxidation at 900°C for 100 h, Al_2O_3 formed on the $Fe_{30}Ni_{25}Cr_{20}Co_{15}Al_{10}$ alloy besides $Cr_{13}Fe_7O_{30}$. The X-ray diffraction pattern for the scale surface had no $NiCr_2O_4$ reflections since spinel separated from the scale surface after the thin continuous Al_2O_3 layer formed (being typical of the oxidation of Ni–Cr–Al alloys), so reflections from the fcc phase were predominant (Fig. 4d). After further oxidation at 1000°C for 50 h, the phase composition of the scales was similar to that of the oxide films after annealing for the same time at 900°C. In both cases, the X-ray diffraction patterns had reflections of $NiCr_2O_4$, Cr_2O_3, and fcc phase (Fig. 4e, f), but the amounts of phase constituents somewhat differed: the amount of Cr_2O_3 decreased and that of $NiCr_2O_4$ increased (Table 2). This will further improve the high-temperature oxidation resistance of the alloys since diffusion processes slow down significantly in the layer with $NiCr_2O_4$.

Cross-sectional studies of the $Fe_{30}Ni_{25}Cr_{20}Co_{15}Al_{10}$ alloy samples oxidized at 900°C + 1000°C revealed a wide continuous region of a light phase, identified by X-rays as the fcc solid solution, under the oxide film layer. This explains why there are no reflections of the bcc phase in the X-ray diffraction pattern. Hence, the surface layers are structured as follows: scale, fcc solid-solution region, and matrix with bcc + fcc phases.

Since the papers (Lin et al., 2011; Kao et al., 2011; Wang et al., 2014) found differences in the phase composition of the $FeNiCoCrAl_x$ alloys (in particular, for x = 5 and 10 at.% Al) after annealing at 900, 950, and 1100°C, we conducted additional X-ray diffraction and microstructural analyses of the samples' end surfaces after complete grinding of the oxide layers to specify changes in the structure and phase composition of the alloy matrices (Fig. 5).
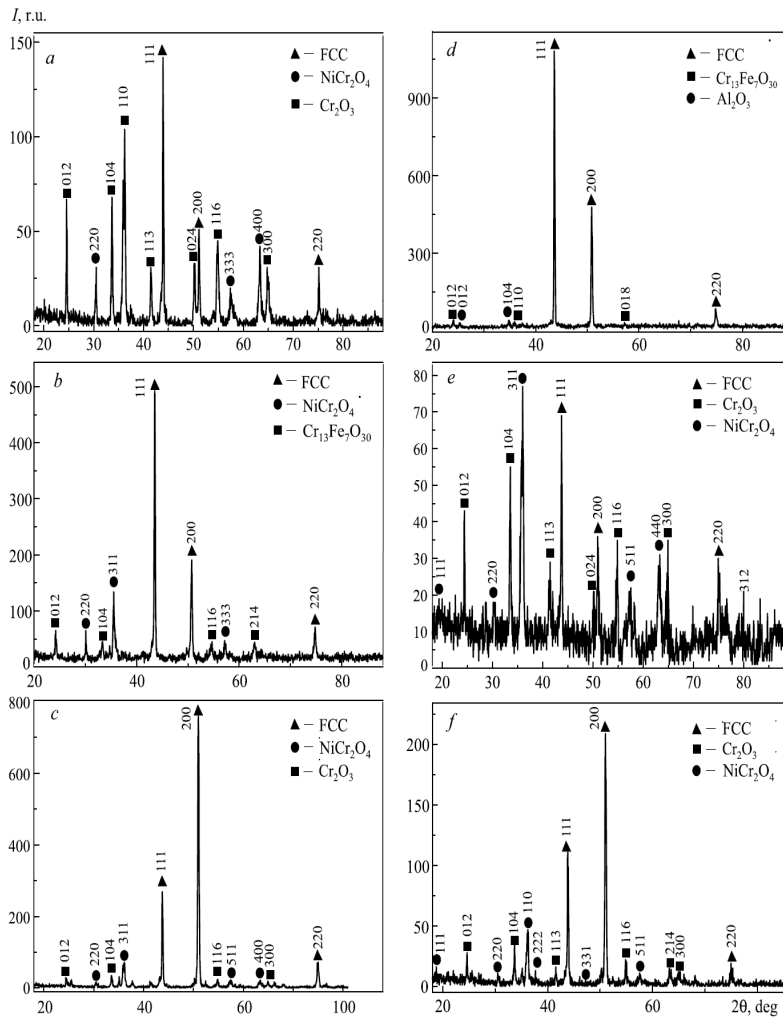
Fig. 4. *X-ray diffraction patterns for the $Fe_{35}Ni_{25}Cr_{20}Co_{20}Al_5$ (a, b, e) and $Fe_{30}Ni_{25}Cr_{20}Co_{15}Al_{10}$ (c, d, f) alloys after oxidation at 900°C for 50 (a, c) and 100 h (b, d) and after oxidation at 1000°C for 50 h (e, f).*

Table 2. *Phase Compositions and Lattice Parameters of Scale Phases after Annealing of the Alloys*

Alloy	Annealing conditions		Phase compositions. wt.%	Lattice parameters. nm	
	$T.$ ºC	$\tau.$ h		A	C
$Fe_{35}Ni_{25}Co_{15}Cr_{20}Al_5$	900	50	7 FCC	0.3577	
			10 $NiCr_2O_4$	0.8306	
			83 $(FeCr)_2O_3$	0.4975	1.3715
	900	100	51 ГЦК	0.3590	
			29 $Cr_{13}Fe_7O_{30}$	0.4986	
			20 $NiCr_2O_4$	0.8350	1.3646
	1000	50	15 FCC	0.3583	
			33 $NiCr_2O_4$	0.8304	
			52 Cr_2O_3	0.4984	1.3597
$Fe_{30}Ni_{25}Co_{15}Cr_{20}Al_{10}$	900	50	41 FCC	0.3585	
			17 $NiCr_2O_4$	0.8299	
			42 Cr_2O_3	0.4958	1.3597
	900	100	92 FCC	0.3580	
			3 $Cr_{13}Fe_7O_{30}$	0.4985	1.3621
			5 Al_2O_3	0.4790	1.3006
	1000	50	43 FCC	0.3597	
			23 $NiCr_2O_4$	0.8318	
			34 Cr_2O_3	0.4990	1.3659
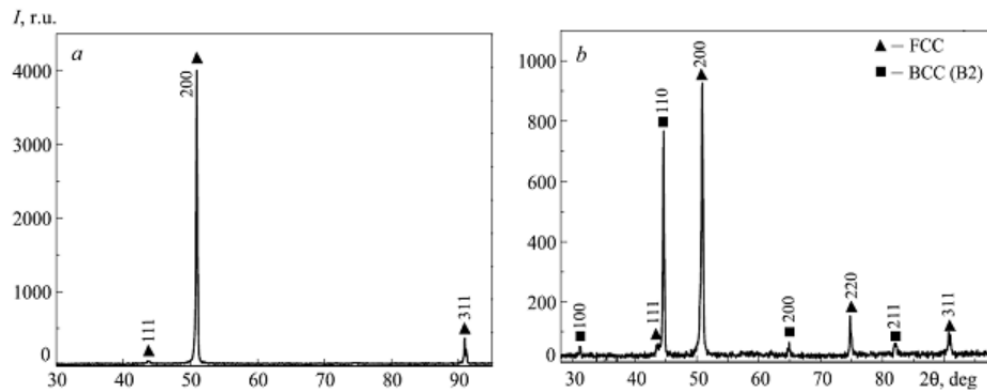
Fig. 5. *X-ray diffraction patterns for the $Fe_{35}Ni_{25}Cr_{20}Co_{20}Al_5$ (a) and $Fe_{30}Ni_{25}Cr_{20}Co_{15}Al_{10}$ (b) alloy matrices after annealing at 900ºC (100 h) and 1000ºC (50 h) and complete removal of the oxide.*

Table 3. *Phase Compositions and Lattice Parameters of Phases in the Alloy Matrix after Annealing at 900℃ for 100h+1000℃ for 50h*

Alloy	Phase constituents	Phase content, %	Lattice parameter a, nm
$Fe_{35}Ni_{25}Cr_{20}Co_{20}Al_5$	FCC	100	0.3586
$Fe_{30}Ni_{25}Cr_{20}Co_{15}Al_{10}$	FCC	46	0.3587
	BCC (B2)	54	0.2870

After annealing at 900°C for 24 h, two phases were found to form in the $FeNiCoCrAl_5$ alloy (Lin et al., 2011): fcc and B2-ordered bcc; at 1100°C, there was only fcc phase, the phase composition of the $Fe_{35}Ni_{25}Cr_{20}Co_{20}Al_5$ alloy remained unchanged after long-term high-temperature annealing in our case; there was only the fcc solid solution. This indicates that this alloy has high thermal stability since variations in line intensities in the X-ray diffraction pattern are not associated with structural changes but result from significant texture confirmed by the respective texture coefficient along the {200} crystallographic direction. For example, this coefficient τ was $0.2775_{(200)}$ after annealing for the alloy with 5 at.% Al and $0.2553_{(200)}$ for the alloy with 10 at.% Al (note that $\tau = 1$ in the absence of texture) (Fig. 5*a*).

The phase composition of the $Fe_{30}Ni_{25}Cr_{20}Co_{15}Al_{10}$ alloy somewhat changed (Fig. 5*b*): the amount of the fcc solid solution sharply decreased from 96 to 46 wt.% and the B2-ordered bcc phase constituted 54 wt.%. Compared to the starting state, the lattice parameter of the fcc phase in the $FeNiCoCrAl_5$ alloy increased from 0.3571 to 0.3586 nm and that of the $FeNiCoCrAl_{10}$ alloy conversely decreased from 0.3603 to 0.3587 nm after long-term high-temperature annealing. The lattice parameter of the bcc solid solution increased to 0.2870 nm. These changes in lattice parameters occur because of diffusion-controlled redistribution of the alloy components (Table 3) among the phase compositions. Microstructural analysis of the annealed $Fe_{35}Ni_{25}Cr_{20}Co_{20}Al_5$ and $Fe_{30}Ni_{25}Cr_{20}Co_{15}Al_{10}$ alloy matrices by scanning electron microscopy (SEM) showed that long-term annealing substantially influenced their morphology. The alloy with 5 at.% Al became homogeneous after annealing, and thus the structure of even a preliminary etched sample was not practically revealed (Fig. 6*a*). The size of dendrites increased and their shape changed in the $Fe_{30}Ni_{25}Cr_{20}Co_{15}Al_{10}$ alloy, while a dark fine phase precipitated within light grains (Fig. 6*b*). The annealed alloy matrix and the distribution of elements in characteristic radiation were studied by SEM, which showed that the dendritic phase was enriched with chromium and iron, cobalt was distributed uniformly between the two phases, and nickel and aluminum were mainly in the space between dendrites and fine phase in the $Fe_{30}Ni_{25}Cr_{20}Co_{15}Al_{10}$ alloy.

The mechanical characteristics of the alloys in cast state and after annealing were determined by automated indentation (Table 4). After annealing, hardness of the $Fe_{35}Ni_{25}Cr_{20}Co_{20}Al_5$ alloy somewhat decreased to 1.8 GPa, which can be attributed to its high homogenization. The elastic modulus sharply reduced to 106 GPa since the lattice parameter of the fcc solid solution increased substantially, which in turn weakened interatomic forces and decreased E.

Table 4. *Mechanical Properties of the Alloys in Starting State and after Long-Term Oxidation at 900℃ for 100 h + 1000℃ for 50 h*

Alloy	Cast state		Matrix after annealing	
	H_{IT}, GPa	E, GPa	H_{IT}, GPa	E, GPa
$Fe_{35}Ni_{25}Cr_{20}Co_{20}Al_5$	2	147	1.8	106
$Fe_{30}Ni_{25}Cr_{20}Co_{15}Al_{10}$	2.5	152	3.1	134
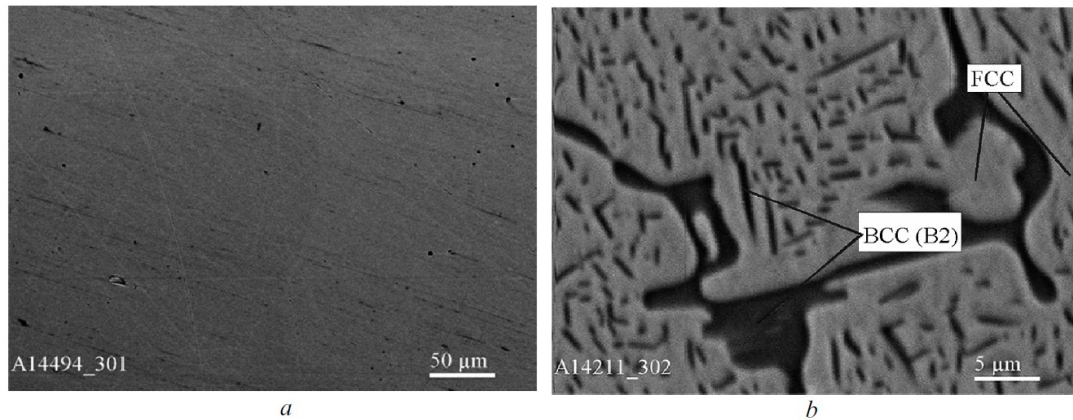
Fig. 6. *Structure of the $Fe_{35}Ni_{25}Cr_{20}Co_{20}Al_5$ (a) and $Fe_{30}Ni_{25}Cr_{20}Co_{15}Al_{10}$ (b) alloy matrices after subsequent annealing at 900℃ + 1000℃.*

The hardness increased to 3.1 GPa in the $Fe_{30}Ni_{25}Cr_{20}Co_{15}Al_{10}$ alloy as the B2-ordered bcc phase formed. This indicates that this alloy is a promising high-temperature oxidation-resistant material.

Summary and conclusion

A series of studies focusing on the cast and annealed alloys in the $Fe_{40-x}NiCoCrAl_x$ system (x = 5 and 10 at.%) has established the following. The starting $Fe_{35}Ni_{25}Cr_{20}Co_{20}Al_5$ alloy is a single-phase fcc solid solution, whose hardness is 2 GPa and elastic modulus 147 GPa. The $Fe_{30}Ni_{25}Cr_{20}Co_{15}Al_{10}$ alloy is two-phase and contains fcc (96%) and bcc (4%) solid solutions. For this reason, it has higher hardness (2.5 GPa) and Young's modulus (152 GPa).

In oxidation at 900°C for 100 h, thin two-phase oxide films that contain $NiCr_2O_4$ spinel and $Cr_{13}Fe_7O_{30}$ oxide form on the $Fe_{35}Ni_{25}Cr_{20}Co_{20}Al_5$ alloy and Al_2O_3 and $Cr_{13}Fe_7O_{30}$ oxides on the $Fe_{30}Ni_{25}Cr_{20}Co_{15}Al_{10}$ alloy. Aluminum oxide in the scale promotes effective protection of the alloy against oxidation. However, when scale annealing temperature increases, Al_2O_3 separates and oxidation proceeds with the formation of $NiCr_2O_4$ and Cr_2O_3 on the surface. Despite this, the high-temperature oxidation resistance of the alloys is at the level of some hightemperature oxidation-resistant alloys in the Ni–Cr–Al system. A wide continuous region of the fcc solid solution under the scale on the $Fe_{30}Ni_{25}Cr_{20}Co_{15}Al_{10}$ alloy has been established to form for the first time.

Long-term high-temperature annealing substantially changes the phase composition and mechanical characteristics of the $Fe_{30}Ni_{25}Cr_{20}Co_{15}Al_{10}$ alloy: the amount of the fcc solid solution sharply decreases to 46 wt.% and an ordered bcc (B2) phase forms. This substantially increases hardness: to 3.1 GPa. This indicates that the $Fe_{30}Ni_{25}Cr_{20}Co_{15}Al_{10}$ alloy is a high-temperature oxidation-resistant material.

Reference

[1] T.M. Butler, M.L. Weaver. Investigation of the phase stabilities in AlNiCoCrFe high-entropy alloys, J. Alloys Compd. 691 (2017) 119-129. https://doi.org/10.1016/j.jallcom.2016.08.121

[2] T.M. Butler, M.L. Weaver. Oxidation behavior of arc-melted AlCoCrFeNi multi-component high-entropy alloys, J. Alloys Compd. 674 (2016) 229-244. https://doi.org/10.1016/j.jallcom.2016.02.257

[3] T.M. Butler, M.L. Weaver, Influence of annealing on the microstructures and oxidation behaviors of Al8(CoCrFeNi)92, Al15(CoCrFeNi)85, and Al30(CoCrFeNi)70 high-entropy alloys, Metals 6 (2016) art.222. https://doi.org/10.3390/met6090222

[4] S.A. Firstov et al. Structural features and solid-solution hardening of the high-entropy CrMnFeCoNi alloy, Powder Metall. Met. Ceram. 55 (2016) 225-235. https://doi.org/10.1007/s11106-016-9797-9

[5] S.A. Firstov et al. Effect of electron density on phase composition of high-entropy equiatomic alloys, Powder Metall. Met. Ceram. 54 (2016) 607-613. https://doi.org/10.1007/s11106-016-9754-7

[6] S.A. Firstov et al. New class of materials – high-entropy alloys and coatings, Vestn. Tomsk. Gos. Univ. 18(4) (2013) 1938-1940.

[7] S.A. Firstov et al. Effect of the crystallization rate on the structure, phase composition, and hardness of the high-entropy AlTiVCrNbMo alloy, Deform. Razrush. Mater. 10 (2013) 8-15.

[8] M.C. Gao, D.E. Alman. Searching for next single-phase high-entropy alloy compositions, Entropy 15 (2013) 4504-4519. https://doi.org/10.3390/e15104504

[9] O. Gumen, I. Selina, R. Selin. Projection of phase composition of lowcost titanium alloy welded joints by finite element mathematical modelling method, Construction of Optimized Energy Potential 12, (2019), 51-56. https://doi.org/10.17512/bozpe.2021.1.07

[10] O. Gumen, I. Bilyk, M. Kruzhkova. Geometrical simulation of optimized vacuum-condensation spraying technology for titanium nitride on structural steel, LNCE 47 (2020) 103-110. https://doi.org/10.1007/978-3-030-27011-7_13

[11] G.R. Holcomb, J. Tylczak, C. Carney. Oxidation of CoCrFeMnNi high-entropy alloys, JOM 67 (2015) 2326-2339. https;//doi.org/10.1007/s11837-015-1517-2

[12] Y.F. Kao, S.K. Chen, T.J. Chen. Electrical, magnetic, and hall properties of $Al_xCoCrFeNi$ high-entropy alloys, J. Alloys Compd. 509 (2011) 1607-1614. https://doi.org/10.1016/j.jallcom.2010.10.210

[13] Y.-K. Kim et al. High-temperature oxidation behavior of Cr–Mn–Fe–Co–Ni high-entropy alloy, Intermetallics 98 (2018) 45-53. https://doi.org/10.1016/j.intermet.2018.04.006

[14] C.M. Lin, H.L. Tsai. Evolution of microstructure, hardness, and corrosion properties of high-entropy Al0.5CoCrFeNi alloy, Intermetallics 19 (2011) 288-294. https://doi.org/10.1016/j.intermet.2010.10.008

[15] S. Guo, C.T. Liu. Phase stability in high-entropy alloys: formation of solid-solution phase or amorphous phase, Prog. Nat. Sci. Mater. Int. 6 (2011) 433-446. https://doi.org/10.1016/S1002-0071(12)60080-X

[16] F.J. Wang et al. Cooling rate and size effect on the microstructure and mechanical properties of AlCoCrFeNi high-entropy alloy, J. Eng. Mater. Technol. 131 (2009) 345011-345013. https://doi.org/10.1115/1.3120387]

[17] W.R. Wang et al. Effects of Al addition on the microstructure and mechanical property of Al$_x$CoCrFeNi high-entropy alloys, Intermetallics 26 (2012) 44-51. https://doi.org/10.1016/j.intermet.2012.03.005

[18] W.R. Wang, W.L Wang, J.W. Yeh, Phases, microstructure and mechanical properties of AlCoCrFeNi high-entropy alloys at elevated temperatures, J. Alloys Compd. 589 (2014) 143-152. https://doi.org/10.1016/j.jallcom.2013.11.084

[19] W. Kai et al. Air-oxidation of FeCoNiCr-based quinary high-entropy alloys at 700–900ºC, Corr. Sci. 121 (2017) 116–125. https://doi.org/10.1016/j.corsci.2017.02.008

[20] J.W. Yeh et al. Nanostructured high-entropy alloys with multiple principal elements: novel alloy design concepts and outcomes, Adv. Eng. Mater. 6 (2004) 299-303. https://doi.org/10.1002/adem.200300567